Available online at www.sciencedirect.com
ScienceDirect
Mathematics and Computers in Simulation 207 (2023) 453–465
MATHEMATICS AND COMPUTERS IN SIMULATION
www.elsevier.com/locate/matcom

Original articles

Stability analysis for a maximum principle preserving explicit scheme of the Allen–Cahn equation

Seokjun Ham, Junseok Kim*

Department of Mathematics, Korea University, Seoul 02841, Republic of Korea

Received 22 August 2022; received in revised form 16 December 2022; accepted 12 January 2023
Available online 18 January 2023

Abstract

In this study, we present the stability analysis of a fully explicit finite difference method (FDM) for solving the Allen–Cahn (AC) equation. The AC equation is a second-order nonlinear partial differential equation (PDE), which describes the antiphase boundaries of the binary phase separation. In the presented stability analysis, we consider the explicit Euler method for the temporal derivative and second-order finite difference in the space direction. The explicit scheme is fast and accurate because it uses a small time step, however, it has a temporal step constraint. We analyze and compute that the explicit time step constraint formula guarantees the discrete maximum principle for the numerical solutions of the AC equation. The numerical stability of the explicit scheme automatically holds when we use the time satisfying the discrete maximum principle. The computational numerical experiments demonstrate the stability, discrete maximum principle, and accuracy of the explicit scheme for the constrained time step. Furthermore, it is shown that the time step obtained is not severe restriction when we consider the temporal accuracy.

Keywords: Allen–Cahn equation; Finite difference method; Fully explicit scheme

1. Introduction

In this paper, we discuss a fully explicit finite difference scheme for numerically solving the Allen–Cahn (AC) equation [2]:

$$\frac{\partial \phi(\mathbf{x},t)}{\partial t} = -\frac{F'(\phi(\mathbf{x},t))}{\epsilon^2} + \Delta\phi(\mathbf{x},t), \quad \mathbf{x}\in\Omega,\ t>0, \tag{1}$$

where $\Omega \subset \mathbb{R}^d$ $(d = 1,2,3)$ is a domain. We apply the homogeneous Neumann boundary condition by $\mathbf{n}\cdot\nabla\phi(\mathbf{x},t) = 0$ on $\partial\Omega$, where $\mathbf{n}$ is an outer unit normal vector on the boundary $\partial\Omega$. Here, $\phi(\mathbf{x},t)$ is difference in concentration of two mixture components, $F(\phi)$ is energy potential, and ϵ is a thickness of interface parameter. The AC equation is derived by the L^2-gradient flow of the following free energy functional:

$$\mathcal{E}(\phi) = \int_\Omega \left(\frac{F(\phi)}{\epsilon^2} + \frac{1}{2}|\nabla\phi|^2\right) d\mathbf{x}. \tag{2}$$

* Corresponding author.
E-mail address: cfdkim@korea.ac.kr (J. Kim).
URL: https://mathematicians.korea.ac.kr/cfdkim/ (J. Kim).

https://doi.org/10.1016/j.matcom.2023.01.016

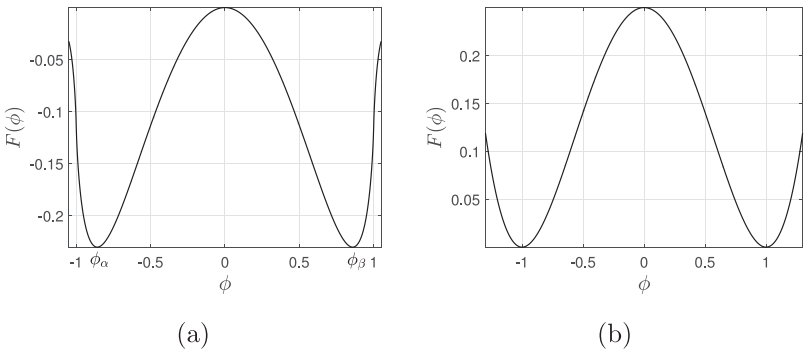

Fig. 1. (a) Logarithmic Flory–Huggins potential energy. (b) Polynomial double-well potential energy.

Energy potential $F(\phi)$ is originally given as the logarithmic Flory–Huggins energy potential:

$$F(\phi) = (1+\phi)\ln(1+\phi) + (1-\phi)\ln(1-\phi) - \frac{\theta_0}{2}\phi^2, \tag{3}$$

where θ_0 is positive constant, which satisfies $\theta_0 > 2$, see [4,6]. However, the logarithmic potential energy is associated with singularity as the phase variable approaches to -1 or 1. For this computational reason, it has typically been approximated by a fourth-order polynomial form:

$$F(\phi) = \frac{1}{4}\left(\phi^2 - 1\right)^2. \tag{4}$$

Figs. 1(a) and (b) illustrate the logarithmic potential energy with $\theta_0 = 3$ and polynomial potential energy, respectively. Here, ϕ_α and ϕ_β are critical points of the logarithmic potential energy. In this study, we focus on the polynomial potential energy in Eq. (4). The AC equation is one of the famous phase field models, which has been applied to model and solve many interesting problems such as two-phase fluid flow [7,33], image inpainting [3,19], image segmentation [18], fingerprint image restoration [21], volume merging [22], thermal-fluid [30,31], crystal growth [20], and copolymer mixtures [11,24], etc.

In general, the exact solution is not available for the AC equation, which is a nonlinear partial differential equation. For this reason, many numerical techniques have been proposed to solve the AC equation. Montanelli and Bootland [25] investigated various exponential integration formulas for the high accuracy of the stiff partial differential equations such as the AC equation. They considered the periodic boundary condition and used Fourier spectral method. Also, there are many stable numerical schemes for the AC equation. Xiao and Feng [32] presented the space–time operator splitting finite element method for the AC equation in multi-phase systems, which preserves a second-order maximum bound principle. Wang et al. [28] proposed a semi-implicit method for the AC equation which is linear, energy stable and maximum principle preserving with double-well potential. The proposed method was superior to the prevalent convex-splitting stabilized scheme. Tang and Yang [26] presented that the stability of the AC equation under the infinity norm can be established for the implicit–explicit scheme in time and space. Joshi and Jaiman [15] presented an adaptive variational method for the conservative and positivity preserving AC equation, which maintains the stable and bounded solution. In [34], an unconditionally stable Fourier-spectral method was presented for the AC equation. The proposed scheme has practical stability, however, it is difficult to apply to the non-uniform grid or adaptive domains as shown in Fig. 2.

Even unconditionally stable numerical schemes should use a sufficiently small time step for the accuracy of the numerical solution. Therefore, there have also been studies on an explicit scheme with high accuracy for the AC equations. Li and Zhang [23] presented an explicit Runge–Kutta scheme with high accuracy and convergence for the AC equation. Aderogba and Chapwanya [1] developed an explicit nonstandard finite difference scheme for the AC equation. The scheme splits the AC equation into the space-independent and time-independent terms, then considers the full equation. In [12], Jeong and Kim proposed an explicit hybrid numerical scheme for the AC equation. Jeong et al. [14] presented a practical adaptive grid method for the AC equation using a discrete narrow band domain. In this perspective, a fully explicit scheme seems to be better. However, the explicit scheme has a time step restriction.

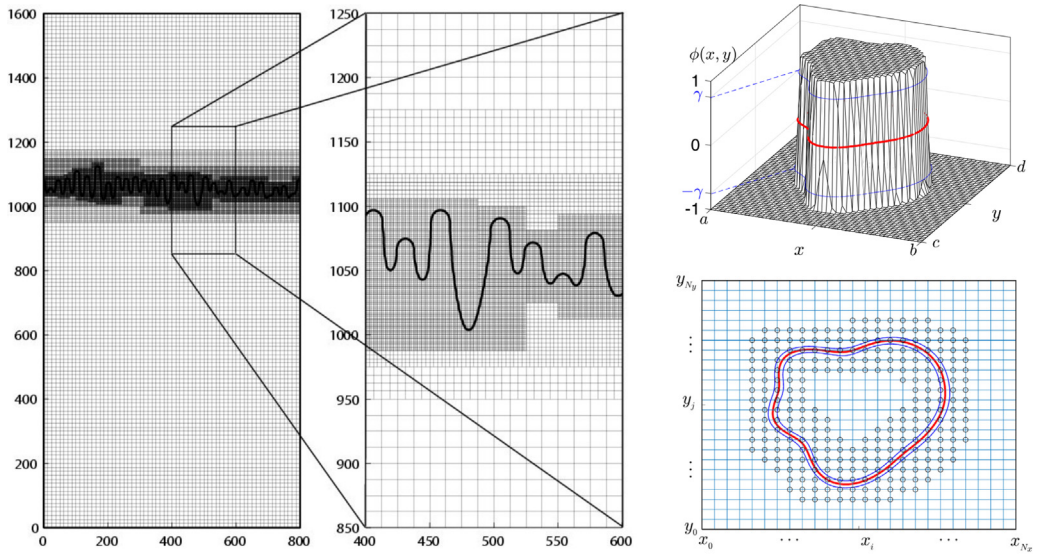

(a) (b)

Fig. 2. (a) Non-uniform mesh (refinement mesh) reprinted from [16] with permission from Springer. (b) Adaptive domain reprinted from [14] with permission from Elsevier.

Fully explicit scheme is a fast and accurate method from the perspective of solving the AC equation. In addition, it is an effective method in applying the adaptive mesh refinement or adaptive domain. Therefore, the stability analysis of the fully explicit scheme solving the AC equation is an important problem. The primary purpose of this paper is to analyze the stability condition and energy stability of the fully explicit scheme for the AC equation. Furthermore, we demonstrate a stability condition by showing various numerical results.

The contents of this paper are organized as follows. In Section 2, we describe the numerical scheme and analyze the time step restriction for the stability of the scheme for the AC equation. We present several numerical experiments in Section 3. Finally, we conclude in Section 4.

2. Numerical scheme and stability analysis

In this section, we consider a fully explicit finite difference scheme for the AC equation. We analyze the time step restriction, which makes the numerical scheme preserve the maximum principle, using the boundedness of the numerical solution. Then, by proving an energy decreasing property, we show the energy stability of the numerical scheme under the analyzed time step.

For a simple description, we consider the AC equation in the one-dimensional (1D) space $\Omega = (L_x, R_x)$. Two- and three-dimensional (2D and 3D) space can be discretized analogously. Let N be the number of spatial grid points, $h = (R_x - L_x)/N$ be the spatial uniform grid size, and discrete computational domain $\Omega_h = \{x_i = L_x + (i - 0.5)h,\ 1 \le i \le N\}$ be the set of cell-centered grid points. We denote the numerical approximations as $\phi_i^n := \phi(x_i, n\Delta t)$, where Δt is the time step size. Time is discretized as $T = N_t \Delta t$, where N_t is the total number of time steps and T is the final time. We define discrete operator ∇_h as $\nabla_h \phi_{i+1/2}^n = (\phi_{i+1}^n - \phi_i^n)/h$. In the discrete computational domain Ω_h, the homogeneous Neumann boundary condition is defined as $\nabla_h \phi_{1/2}^n = \nabla_h \phi_{N+1/2}^n = 0$, for $n = 1, \dots, N_t$. Then, we define a discrete Laplacian operator by $\Delta_h \phi_i^n = (\nabla_h \phi_{i+1/2}^n - \nabla_h \phi_{i-1/2}^n)/h = (\phi_{i-1}^n - 2\phi_i^n + \phi_{i+1}^n)/h^2$. We denote the discrete maximum norm by $\|\boldsymbol{\phi}^n\|_\infty = \max_{1 \le i \le N} |\phi_i^n|$, where $\boldsymbol{\phi}^n = (\phi_1^n, \phi_2^n, \cdots, \phi_N^n)$. The AC equation (1) can be expressed with the following convergence accuracies in time and space:

$$\begin{aligned} \frac{\phi_i^{n+1} - \phi_i^n}{\Delta t} + \mathcal{O}(\Delta t) &= -\frac{(\phi_i^n)^3 - \phi_i^n}{\epsilon^2} + \Delta_h \phi_i^n + \mathcal{O}(h^2) \\ &= \frac{\phi_i^n - (\phi_i^n)^3}{\epsilon^2} + \frac{\phi_{i-1}^n - 2\phi_i^n + \phi_{i+1}^n}{h^2} + \mathcal{O}(h^2). \end{aligned} \tag{5}$$

Then, the AC equation (1) is approximated by the following in a fully explicit scheme.

$$\frac{\phi_i^{n+1}-\phi_i^n}{\Delta t}=\frac{\phi_i^n-(\phi_i^n)^3}{\epsilon^2}+\frac{\phi_{i-1}^n-2\phi_i^n+\phi_{i+1}^n}{h^2}. \tag{6}$$

Theorem 1. *Assume that the initial condition satisfies* $\max_{1\le i\le N}|\phi_i^0|\le 1$. *Then, the fully explicit scheme (6) preserves the boundedness of the numerical solution*

$$|\phi_i^{n+1}|\le 1,\quad \text{for}\ \ 1\le i\le N,\ n\ge 0, \tag{7}$$

if the time step satisfies

$$\Delta t\le\frac{\epsilon^2h^2}{2h^2+2\epsilon^2}. \tag{8}$$

Proof. The fully explicit scheme for the AC equation (6) can be rewritten as

$$\phi_i^{n+1}=\phi_i^n+\Delta t\left(\frac{\phi_i^n-(\phi_i^n)^3}{\epsilon^2}+\frac{\phi_{i-1}^n-2\phi_i^n+\phi_{i+1}^n}{h^2}\right). \tag{9}$$

We prove this theorem using the conditions that satisfy the following bounds of the numerical solution $|\phi_i^{n+1}|\le 1$. We divide the proof into four cases.

Case 1. $\phi_i^n=0$

The numerical solution (9) is bounded as

$$\left|\phi_i^{n+1}\right|=\left|\Delta t\frac{\phi_{i-1}^n+\phi_{i+1}^n}{h^2}\right|\le\frac{2\Delta t}{h^2}, \tag{10}$$

which satisfies $|\phi_i^{n+1}|\le 1$ provided $\Delta t\le h^2/2$.

Case 2. $\phi_i^n=1$

The numerical solution (9) is rewritten as

$$\phi_i^{n+1}=1+\Delta t\frac{\phi_{i-1}^n-2+\phi_{i+1}^n}{h^2}. \tag{11}$$

Because $\phi_{i-1}^n-2+\phi_{i+1}^n\le 0$, we have $\phi_i^{n+1}\le 1$. If $\phi_{i-1}^n-2+\phi_{i+1}^n=0$, there is no constraint for the time step; otherwise, i.e., $\phi_{i-1}^n-2+\phi_{i+1}^n<0$, then $\Delta t\le h^2/2$ results in $\phi_i^{n+1}\ge -1$. Therefore, we have $|\phi_i^{n+1}|\le 1$.

Case 3. $0<\phi_i^n<1$

In Eq. (9), if $\frac{\phi_i^n-(\phi_i^n)^3}{\epsilon^2}+\frac{\phi_{i-1}^n-2\phi_i^n+\phi_{i+1}^n}{h^2}\ge 0$, then we have $-1\le\phi_i^{n+1}$. From Eq. (9), we can obtain the following inequality.

$$\phi_i^{n+1}\le\phi_i^n+\Delta t\left(\frac{\phi_i^n-(\phi_i^n)^3}{\epsilon^2}+\frac{2-2\phi_i^n}{h^2}\right). \tag{12}$$

We want to find the condition of Δt satisfying that

$$\phi_i^n+\Delta t\left(\frac{\phi_i^n-(\phi_i^n)^3}{\epsilon^2}+\frac{2-2\phi_i^n}{h^2}\right)\le 1. \tag{13}$$

Then, it can be rewritten as

$$\Delta t(1-\phi_i^n)\left(\frac{\phi_i^n(1+\phi_i^n)}{\epsilon^2}+\frac{2}{h^2}\right)\le 1-\phi_i^n. \tag{14}$$

By dividing both sides of (14) by $(1-\phi_i^n)>0$, we have

$$\Delta t\left(\frac{\phi_i^n(1+\phi_i^n)}{\epsilon^2}+\frac{2}{h^2}\right)\le 1. \tag{15}$$

Therefore, Δt has the following constraint.

$$\Delta t \leq \frac{\epsilon^2 h^2}{h^2 \phi_i^n (1+\phi_i^n) + 2\epsilon^2}. \tag{16}$$

Here, because $0 < \phi_i^n(1+\phi_i^n) < 2$, we obtain the following condition.

$$\Delta t \leq \frac{\epsilon^2 h^2}{2h^2 + 2\epsilon^2}. \tag{17}$$

Hence, when $\Delta t \leq \epsilon^2 h^2/(2h^2+2\epsilon^2)$, we have $|\phi_i^{n+1}| \leq 1$.

From Eq. (9), when $\frac{\phi_i^n - (\phi_i^n)^3}{\epsilon^2} + \frac{\phi_{i-1}^n - 2\phi_i^n + \phi_{i+1}^n}{h^2} < 0$, then $\phi_i^{n+1} \leq 1$ always holds true. From Eq. (9), we have the following inequality.

$$\phi_i^n + \Delta t \left(\frac{\phi_i^n - (\phi_i^n)^3}{\epsilon^2} - \frac{2+2\phi_i^n}{h^2} \right) \leq \phi_i^{n+1}. \tag{18}$$

From the inequality (18), to satisfy that $-1 \leq \phi_i^{n+1}$, we consider the following inequality.

$$-1 \leq \phi_i^n + (1+\phi_i^n)\Delta t \left(\frac{\phi_i^n(1-\phi_i^n)}{\epsilon^2} - \frac{2}{h^2} \right). \tag{19}$$

It can be rewritten as

$$-1 \leq \Delta t \left(\frac{\phi_i^n(1-\phi_i^n)}{\epsilon^2} - \frac{2}{h^2} \right). \tag{20}$$

Then, we have

$$\frac{\epsilon^2 h^2}{2\epsilon^2 - h^2 \phi_i^n (1-\phi_i^n)} \geq \Delta t. \tag{21}$$

Because $\phi_i^n(1-\phi_i^n) > 0$, we obtain the following condition.

$$\Delta t \leq \frac{h^2}{2}. \tag{22}$$

Therefore, $\Delta t \leq h^2/2$ results in $|u_i^{n+1}| \leq 1$.

Case 4. $-1 \leq \phi_i^n < 0$

When $-1 \leq \phi_i^n < 0$, it also can be written as $0 < -\phi_i^n \leq 1$. Multiplying both sides of Eq. (9) by -1, we get

$$-\phi_i^{n+1} = -\phi_i^n - \Delta t \left(\frac{\phi_i^n - (\phi_i^n)^3}{\epsilon^2} + \frac{\phi_{i-1}^n - 2\phi_i^n + \phi_{i+1}^n}{h^2} \right) \tag{23}$$

$$= -\phi_i^n + \Delta t \left(\frac{(-\phi_i^n) - (-\phi_i^n)^3}{\epsilon^2} + \frac{-\phi_{i-1}^n - (-2\phi_i^n) - \phi_{i+1}^n}{h^2} \right). \tag{24}$$

Considering the right side of Eq. (24) for $-\phi_i^n$, we can apply the proofs of Cases 2 and 3. By the results of Cases 2 and 3, it can be proved that $\Delta t \leq \epsilon^2 h^2/(2h^2+2\epsilon^2)$ guarantees $|\phi_i^{n+1}| = |-\phi_i^{n+1}| \leq 1$. Because $\epsilon^2 h^2/(2h^2+2\epsilon^2) < h^2/2$ for $h > 0$, the proof of this theorem is ended. □

In the same way, Theorem 1 can be extended to higher-dimensional spaces. Table 1 lists the time step restrictions of the fully explicit scheme for the AC equation in one-, two-, and three-dimensional (1D, 2D, and 3D) spaces for each case. We can derive the time step restriction $\Delta t(h, \epsilon, d)$ for each dimension ($d = 1, 2$, and 3) as

$$\Delta t(h, \epsilon, d) = \frac{\epsilon^2 h^2}{2h^2 + 2d\epsilon^2}. \tag{25}$$

From the result of stability analysis (25), Fig. 3 illustrates the time step constraint of the explicit scheme to the AC equation for ϵ in 1D, 2D, and 3D spaces, here $h = 1/64$ is used. The explicit scheme for the heat equation has the time step constraint as $\Delta t \leq 0.5h^2/d$ for dimension $d = 1, 2, 3$. Fig. 3 shows that for the explicit scheme, the time step restriction of the AC equation is smaller than that of the heat equation. We note that $\epsilon \approx h$ has been used

Table 1
Time step restrictions for one-, two-, and three-dimensional spaces.

	1D	2D	3D
Case 1	$h^2/2$	$h^2/4$	$h^2/6$
Case 2	$h^2/2$	$h^2/4$	$h^2/6$
Case 3	$\epsilon^2h^2/(2h^2+2\epsilon^2)$	$\epsilon^2h^2/(2h^2+4\epsilon^2)$	$\epsilon^2h^2/(2h^2+6\epsilon^2)$
Case 4	$\epsilon^2h^2/(2h^2+2\epsilon^2)$	$\epsilon^2h^2/(2h^2+4\epsilon^2)$	$\epsilon^2h^2/(2h^2+6\epsilon^2)$
Minimum	$\epsilon^2h^2/(2h^2+2\epsilon^2)$	$\epsilon^2h^2/(2h^2+4\epsilon^2)$	$\epsilon^2h^2/(2h^2+6\epsilon^2)$

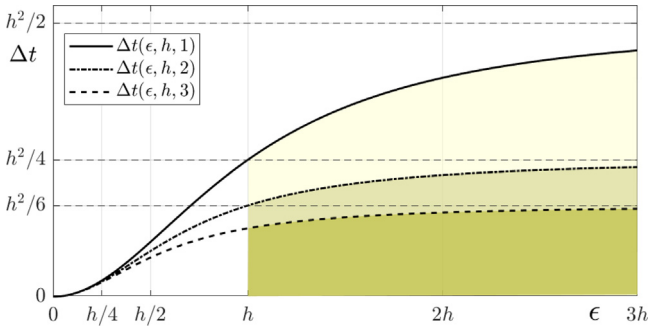

Fig. 3. Time step constraint for ϵ, here $h = 1/64$ is used.

in most of numerical simulations. As shown in Fig. 3, the time step restriction is practically $\Delta t \le 0.5h^2/(d+1)$ for dimension $d = 1, 2, 3$.

Remark 1. When the double-well energy potential is replaced by the Flory–Huggins logarithmic potential, for $\phi_\alpha \le \phi \le \phi_\beta$, the bound estimate can be made with the positive boundedness of the time step restriction as in the case of the polynomial double-well potential. Here, $-1 < \phi_\alpha < 0$ and $0 < \phi_\beta < 1$ are critical points of the Flory–Huggins logarithmic potential.

2.1. Energy stability analysis

In this section, we analyze the energy stability of the fully explicit scheme for the AC equation under the proposed time step constraint (25) on 1D space ($d = 1$). The analysis below follows the similar process in [13]. First, we define a discrete l_2-inner product by

$$\langle \boldsymbol{\phi}, \boldsymbol{\psi} \rangle_h = h \sum_{i=1}^{N} \phi_i \psi_i. \tag{26}$$

From the free energy functional (2), we define a discrete energy functional,

$$\mathcal{E}_h(\boldsymbol{\phi}^n) = \frac{h}{4\epsilon^2} \sum_{i=1}^{N} ((\phi_i^n)^2 - 1)^2 + \frac{h}{2} \sum_{i=1}^{N-1} \left| \nabla_h \phi^n_{i+\frac{1}{2}} \right|^2. \tag{27}$$

We decompose the discrete energy functional $\mathcal{E}_h(\boldsymbol{\phi}^n)$ into two parts as

$$\mathcal{E}_h(\boldsymbol{\phi}^n) = \mathcal{E}^{(1)}(\boldsymbol{\phi}^n) + \mathcal{E}^{(2)}(\boldsymbol{\phi}^n), \tag{28}$$

where

$$\mathcal{E}^{(1)}(\boldsymbol{\phi}^n) = \frac{h}{4\epsilon^2} \sum_{i=1}^{N} ((\phi_i^n)^2 - 1)^2 \quad \text{and} \quad \mathcal{E}^{(2)}(\boldsymbol{\phi}^n) = \frac{h}{2} \sum_{i=1}^{N-1} \left| \nabla_h \phi^n_{i+\frac{1}{2}} \right|^2. \tag{29}$$

Then, the fully explicit scheme for the AC equation can be formed as a gradient of discrete total energy as follows:

$$\frac{\phi_i^{n+1}-\phi_i^n}{\Delta t} = -\frac{1}{h}\nabla\mathcal{E}_h(\boldsymbol{\phi}^n)_i, \quad \text{for } i = 1,\dots,N. \tag{30}$$

Given the discrete energy functionals $\mathcal{E}^{(1)}(\boldsymbol{\phi})$ and $\mathcal{E}^{(2)}(\boldsymbol{\phi})$, we define the Hessian matrix $\mathbf{H}^{(1)}$ and $\mathbf{H}^{(2)}$ as the Jacobian of the $\nabla\mathcal{E}^{(1)}(\boldsymbol{\phi})$ and $\nabla\mathcal{E}^{(2)}(\boldsymbol{\phi})$, respectively. Then, the Hessian matrix is defined as

$$\begin{aligned}
&\left\{\mathbf{H}^{(1)}, \mathbf{H}^{(2)}\right\} \\
&= \left\{\nabla^2\mathcal{E}^{(1)}(\boldsymbol{\phi}), \nabla^2\mathcal{E}^{(2)}(\boldsymbol{\phi})\right\} \\
&= \left\{ \frac{h}{\epsilon^2}\begin{pmatrix} 3\phi_1^2-1 & & & & 0 \\ & 3\phi_2^2-1 & & & \\ & & \ddots & & \\ & & & 3\phi_{N-1}^2-1 & \\ 0 & & & & 3\phi_N^2-1 \end{pmatrix}, h\begin{pmatrix} 1 & -1 & & & 0 \\ -1 & 2 & -1 & & \\ & \ddots & \ddots & \ddots & \\ & & -1 & 2 & -1 \\ 0 & & & -1 & 1 \end{pmatrix} \right\},
\end{aligned}$$

where we use the homogeneous Neumann boundary condition. Here, the eigenvalues of $\mathbf{H}^{(1)}$ and $\mathbf{H}^{(2)}$ are

$$\lambda_k^{(1)} = \frac{h}{\epsilon^2}(3\phi_k^2-1), \quad \lambda_k^{(2)} = \frac{4}{h}\sin^2\frac{(k-1)\pi}{2N}, \tag{31}$$

for $k = 1, 2, \dots, N$, respectively. Let $\mathbf{v}_k = \mathbf{w}_k/|\mathbf{w}_k|$ be the orthonormal eigenvector corresponding to the eigenvalues $\lambda_k^{(2)}$, where

$$\mathbf{w}_k = \left(\cos\frac{(k-1)\pi}{2N}, \cos\frac{3(k-1)\pi}{2N}, \dots, \frac{(2N-1)(k-1)\pi}{2N}\right).$$

Then, we can express $\boldsymbol{\phi}^{n+1}-\boldsymbol{\phi}^n$ with terms of $\mathbf{v}_k$ as

$$\boldsymbol{\phi}^{n+1}-\boldsymbol{\phi}^n = \sum_{k=1}^{N} c_k\mathbf{v}_k. \tag{32}$$

Theorem 2. *Let us consider the AC equation with homogeneous Neumann boundary condition. If the initial condition is bounded by 1, i.e.,* $\max_{1\le i\le N}|\phi_i^0| \le 1$*, then the numerical solutions obtained by the fully explicit scheme* (6) *satisfy the discrete energy decreasing property:*

$$\mathcal{E}_h(\boldsymbol{\phi}^{n+1}) \le \mathcal{E}_h(\boldsymbol{\phi}^n), \tag{33}$$

provided that the time step satisfies

$$\Delta t \le \frac{\epsilon^2 h^2}{2h^2+2\epsilon^2}. \tag{34}$$

Proof. $\mathcal{E}_h(\boldsymbol{\phi}^{n+1})$ can be expressed by the Taylor expansion at $\boldsymbol{\phi}^n$ up to second order as

$$\mathcal{E}_h(\boldsymbol{\phi}^{n+1}) = \mathcal{E}_h(\boldsymbol{\phi}^n) + \left\langle \frac{1}{h}\nabla\mathcal{E}_h(\boldsymbol{\phi}^n), \boldsymbol{\phi}^{n+1}-\boldsymbol{\phi}^n \right\rangle_h \tag{35}$$

$$+ \left\langle \frac{1}{2h}\nabla^2\mathcal{E}_h(\xi)(\boldsymbol{\phi}^{n+1}-\boldsymbol{\phi}^n), \boldsymbol{\phi}^{n+1}-\boldsymbol{\phi}^n \right\rangle_h, \tag{36}$$

where $\xi = \alpha\boldsymbol{\phi}^n + (1-\alpha)\boldsymbol{\phi}^{n+1}$ and $0 \le \alpha \le 1$. Then, we have the following equation,

$$\begin{aligned}
\mathcal{E}_h(\boldsymbol{\phi}^{n+1}) - \mathcal{E}_h(\boldsymbol{\phi}^n) &= \left\langle \frac{1}{h}\nabla\mathcal{E}_h(\boldsymbol{\phi}^n), \boldsymbol{\phi}^{n+1}-\boldsymbol{\phi}^n \right\rangle_h \\
&+ \left\langle \frac{1}{2h}\nabla^2\mathcal{E}_h(\xi)(\boldsymbol{\phi}^{n+1}-\boldsymbol{\phi}^n), \boldsymbol{\phi}^{n+1}-\boldsymbol{\phi}^n \right\rangle_h.
\end{aligned} \tag{37}$$

By using Eq. (30) and the Hessian matrix, Eq. (37) can be converted to

$$\begin{aligned}
&\mathcal{E}_h(\boldsymbol{\phi}^{n+1}) - \mathcal{E}_h(\boldsymbol{\phi}^n) \\
&= -\left\langle \frac{\boldsymbol{\phi}^{n+1}-\boldsymbol{\phi}^n}{\Delta t}, \boldsymbol{\phi}^{n+1}-\boldsymbol{\phi}^n \right\rangle_h + \left\langle \frac{1}{2h}\left(\mathbf{H}^{(1)}+\mathbf{H}^{(2)}\right)(\boldsymbol{\phi}^{n+1}-\boldsymbol{\phi}^n), \boldsymbol{\phi}^{n+1}-\boldsymbol{\phi}^n \right\rangle_h \\
&= \left\langle \left[\frac{1}{2h}\left(\mathbf{H}^{(1)}+\mathbf{H}^{(2)}\right) - \frac{1}{\Delta t}\right](\boldsymbol{\phi}^{n+1}-\boldsymbol{\phi}^n), \boldsymbol{\phi}^{n+1}-\boldsymbol{\phi}^n \right\rangle_h \\
&= \sum_{k,l=1}^{N} \left\langle \left[\frac{1}{2h}\lambda_k^{(1)} + \frac{1}{2h}\lambda_k^{(2)} - \frac{1}{\Delta t}\right] c_k\mathbf{v}_k, c_l\mathbf{v}_l \right\rangle_h \\
&= \sum_{k,l=1}^{N} \left\langle \left[\frac{1}{2\epsilon^2}(3\eta_k^2-1) + \frac{2}{h^2}\sin^2\frac{(k-1)\pi}{2N} - \frac{1}{\Delta t}\right] c_k\mathbf{v}_k, c_l\mathbf{v}_l \right\rangle_h \\
&= \sum_{k=1}^{N} \left[\frac{1}{2\epsilon^2}(3\eta_k^2-1) + \frac{2}{h^2}\sin^2\frac{(k-1)\pi}{2N} - \frac{1}{\Delta t}\right] {c_k}^2,
\end{aligned} \tag{38}$$

where $\eta_k = \alpha\phi_k^n + (1-\alpha)\phi_k^{n+1}$ and $0 \le \alpha \le 1$. By Theorem 1, we note that $|\eta_k| \le 1$ with time step condition (34), for $1 \le k \le N$. If $\Delta t \le \epsilon^2 h^2/(2h^2+2\epsilon^2)$, then we can derive the following inequality from Eq. (38):

$$\mathcal{E}_h(\boldsymbol{\phi}^{n+1}) - \mathcal{E}_h(\boldsymbol{\phi}^n) \le \sum_{k=1}^{N} {c_k}^2 \left[\frac{1}{\epsilon^2} + \frac{2}{h^2} - \frac{2h^2+2\epsilon^2}{\epsilon^2 h^2}\right] = -\frac{{c_k}^2 N}{\epsilon^2} < 0.$$

The proof of this theorem is ended. □

We note that there is a time step restriction, $\Delta t \le \epsilon^2 h^2/(2h^2+2\epsilon^2)$, for the energy stability unlike an unconditionally stable implicit scheme [30].

3. Computational tests

We conduct computational experiments to demonstrate the stability of the explicit scheme for the AC equation. In 1D space, the homogeneous Neumann boundary condition is implemented as

$$\phi_0 = \phi_1 \quad \text{and} \quad \phi_{N+1} = \phi_N. \tag{39}$$

It applies to 2D and 3D space, similarly. We use the interfacial transition thickness parameter $\epsilon_m = mh/[2\sqrt{2}\tanh^{-1}(0.9)]$, which makes the thickness of the interfacial transition layer approximately mh for some positive integer m, see [5]. For the following tests, we use $\epsilon = \epsilon_m$ for appropriate m.

3.1. Convergence of numerical solutions

In this test, we use the traveling wave benchmark solution, which is one of the exact solutions of the AC equation [5,29]:

$$\phi_{exact}(x,t) = \frac{1}{2}\left[1 - \tanh\left(\frac{x - 3t/(\sqrt{2}\epsilon)}{2\sqrt{2}\epsilon}\right)\right]. \tag{40}$$

We investigate the convergence of the solution using the stable condition of time step $\Delta t(h,\epsilon,1) = \epsilon^2 h^2/(2h^2+2\epsilon^2)$. In Fig. 4, we use four different time step sizes $\Delta t = \Delta t(h,\epsilon,1)$, $0.5\Delta t(h,\epsilon,1)$, $0.25\Delta t(h,\epsilon,1)$, and $0.125\Delta t(h,\epsilon,1)$ on computational domain $\Omega = (-0.5, 1.5)$. Here, the other parameters are used as $N = 400$, $h = 0.005$, $\epsilon = \epsilon_{10}$, and $T = 500\Delta t(h,\epsilon,1)$.

To estimate the temporal convergence rate of the explicit scheme for the AC equation, we refine recursively the time step in half. We define a discrete error of numerical solution as $\mathbf{e}^{N_t} = (e_1^{N_t}, e_2^{N_t}, \ldots, e_N^{N_t})$, where $e_i^{N_t} = \phi_i^{N_t} - \phi_{exact}(x_i, N_t\Delta t)$. We define l_2-error as $\|\mathbf{e}^{N_t}\|_2 = \sqrt{h\sum_{i=1}^{N}(e_i^{N_t})^2}$ and max-error as $\|\mathbf{e}^{N_t}\|_{max} = \max_{1\le i\le N}|e_i^{N_t}|$. Let $\log_2(\|\mathbf{e}^{N_t}\|/\|\mathbf{e}^{2N_t}\|)$ be a time convergence rate. Table 2 lists errors and temporal convergence rates for l_2- and max-error. It confirms that the scheme is stable with the analyzed time steps and has first-order accuracy in time.

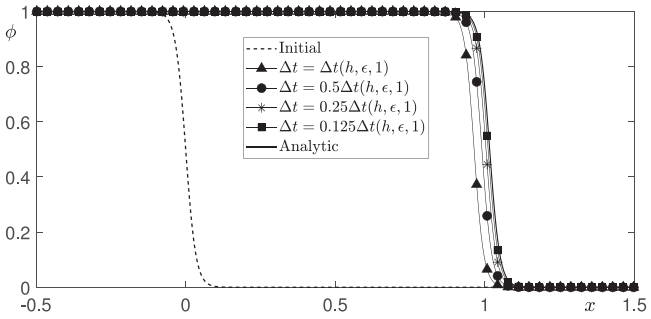

Fig. 4. Numerical solution of traveling wave for the AC equation at $t = T$ with initial and analytic profiles, $\phi_{exact}(x, 0)$ and $\phi_{exact}(x, T)$, respectively. Here $\epsilon = \epsilon_{10}$.

Table 2
Time errors and convergence rates at $t = T$.

Δt	$\Delta t(h, \epsilon, 1)$		$\Delta t(h, \epsilon, 1)/2$		$\Delta t(h, \epsilon, 1)/4$		$\Delta t(h, \epsilon, 1)/8$
l_2-error	0.1531		0.0801		0.0382		0.0162
rate		0.9349		1.0692		1.2395	
max-error	0.6527		0.3687		0.1788		0.0762
rate		0.8239		1.0442		1.2302	

3.2. Accuracy comparison with Fourier-spectral method

In [34], an unconditionally stable Fourier-spectral method (FSM) was presented for the AC equation using discrete Fourier transform with periodic boundary condition. In this section, we compare the accuracy of the fully explicit scheme and unconditionally stable FSM. We use discrete cosine transform (DCT) and inverse discrete cosine transform (IDCT) to apply the homogeneous Neumann boundary condition. For the given data ϕ_i^n for $i = 1, \ldots, N$ and some n, the DCT and IDCT are defined as follows:

$$\hat{\phi}_p^n = \alpha_p \sum_{i=1}^{N} \phi_i^n \cos(\xi_p \pi x_i), \tag{41}$$

$$\phi_i^n = \sum_{p=1}^{N} \alpha_p \hat{\phi}_p^n \cos(\xi_p \pi x_i), \tag{42}$$

respectively, where $\alpha_1 = \sqrt{1/N}$, $\alpha_p = \sqrt{2/N}$ for $p \geq 2$, and $\xi_p = (p-1)/L$ for $p = 1, \ldots, N$. In [34], the authors applied the linearly stabilized splitting scheme to solve the AC equation (1). In 1D space, the numerical scheme is as follows.

$$\frac{\phi_i^{n+1} - \phi_i^n}{\Delta t} = -\frac{2\phi_i^{n+1} + f(\phi_i^n)}{\epsilon^2} + \Delta\phi_i^{n+1}, \tag{43}$$

where $f(\phi) = \phi^3 - 3\phi$. In the discrete Fourier space, Eq. (43) can be transformed as follows:

$$\frac{\hat{\phi}_p^{n+1} - \hat{\phi}_i\, p^n}{\Delta t} = -\frac{2\hat{\phi}_p^{n+1} + \hat{f}_p^n}{\epsilon^2} - \pi^2\xi^2\hat{\phi}_p^{n+1}. \tag{44}$$

Then, we obtain the following solution in discrete Fourier space

$$\hat{\phi}_p^{n+1} = \frac{\epsilon^2\hat{\phi}_p^n - \Delta t\, \hat{f}_p^n}{\epsilon^2 + \Delta t(2 + \pi^2\xi^2\epsilon^2)}. \tag{45}$$

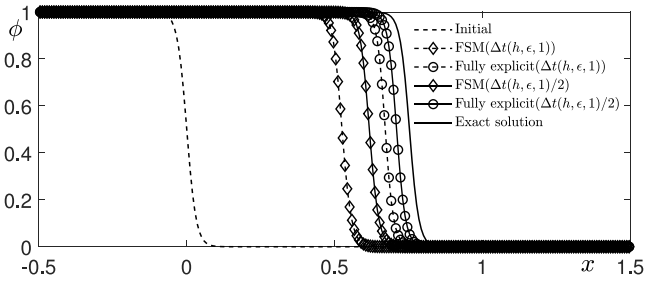

Fig. 5. Comparison of numerical traveling wave solutions using the fully explicit scheme and FSM at $t = T$. Here, $\epsilon = \epsilon_6$ is used.

Table 3
l_2-errors for fully explicit scheme and FSM.

Case	Fully explicit	FSM
$\Delta t = \Delta t(h, \epsilon, 1)$	0.2330	0.4451
$\Delta t = \Delta t(h, \epsilon, 1)/2$	0.1343	0.3218

Finally, we can obtain the numerical solution ϕ_i^{n+1} using IDCT (42):

$$\phi_i^{n+1} = \sum_{p=1}^{N} \alpha_p \hat{\phi}_p^{n+1} \cos(\xi_p \pi x_i). \tag{46}$$

In Fig. 5, we compare the numerical traveling wave solutions of the AC equation using the fully explicit scheme and FSM. We use an initial profile $\phi(x, 0) = 0.5\left[1 - \tanh\left(x/(2\sqrt{2}\epsilon)\right)\right]$ in $\Omega = (-0.5, 1.5)$, where $\epsilon = \epsilon_6$. Here, the numerical parameters are used as $N = 256$, $h = 2/N$, and $T = 0.004$. From the result in Fig. 5, l_2-errors for fully explicit scheme and FSM are listed in Table 3.

FSM is stable even with large time steps, however, it is less accurate. From the result in Fig. 5, for the same time step, it can be seen that the fully explicit scheme is more accurate than the FSM.

3.3. Motion by mean curvature

The zero level interface of solution to the AC equation follows the mean curvature flow, as $\epsilon \to 0$ [17]. In this section, we investigate the mean curvature flow of the numerical solution to the AC equation obtained by the fully explicit scheme with the restricted time step $\Delta t = \Delta t_d$, where Δt_d is defined in Eq. (25). To demonstrate that the scheme is stable using the analyzed time steps, we observe the temporal evolution of the solutions and confirm properties of the AC equation. In the following tests, we use the thickness of interface parameter $\epsilon = \epsilon_{10}$.

In 2D computational domain $\Omega = (-1, 1) \times (-1, 1)$, we use an 128×128 mesh grid, $h = 1/64$, and time step $\Delta t(h, \epsilon, 2) = \epsilon^2 h^2/(2h^2 + 4\epsilon^2)$. The initial condition is given as

$$\phi(x, y, 0) = \tanh\left(\frac{R_0 - \sqrt{x^2 + y^2}}{\sqrt{2}\epsilon}\right), \tag{47}$$

where $R_0 = 0.7$, as shown in Fig. 6(a). The analytic radius is given as $R(t) = \sqrt{R_0^2 - 2t}$ [12]. Figs. 6(a)–(c) show the temporal evolution of the numerical solutions and Fig. 6(d) illustrates analytic and numerical radii over time t.

We conduct a similar computational experiment in 3D domain $\Omega = (-1, 1) \times (-1, 1) \times (-1, 1)$. We use an $128 \times 128 \times 128$ mesh, $h = 1/64$, and time step $\Delta t(h, \epsilon, 3) = \epsilon^2 h^2 / \left(2h^2 + 6\epsilon^2\right)$. The initial condition is given as

$$\phi(x, y, z, 0) = \tanh\left(\frac{R_0 - \sqrt{x^2 + y^2 + z^2}}{\sqrt{2}\epsilon}\right), \tag{48}$$

where we use $R_0 = 0.7$. The analytic radius is $R(t) = \sqrt{R_0 - 4t}$ in 3D space [12]. Figs. 7(a)–(c) show the temporal evolution of zero level isosurface of solution for the AC equation and Fig. 7(d) illustrates analytic and numerical

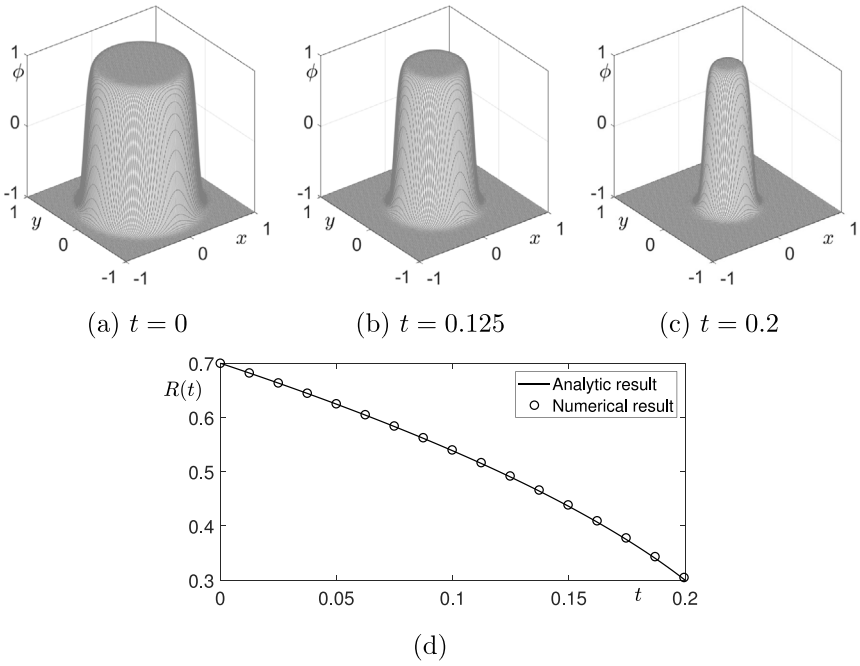

Fig. 6. (a)–(c) Temporal evolution of numerical solutions. (d) Analytic and numerical radius changes over time.

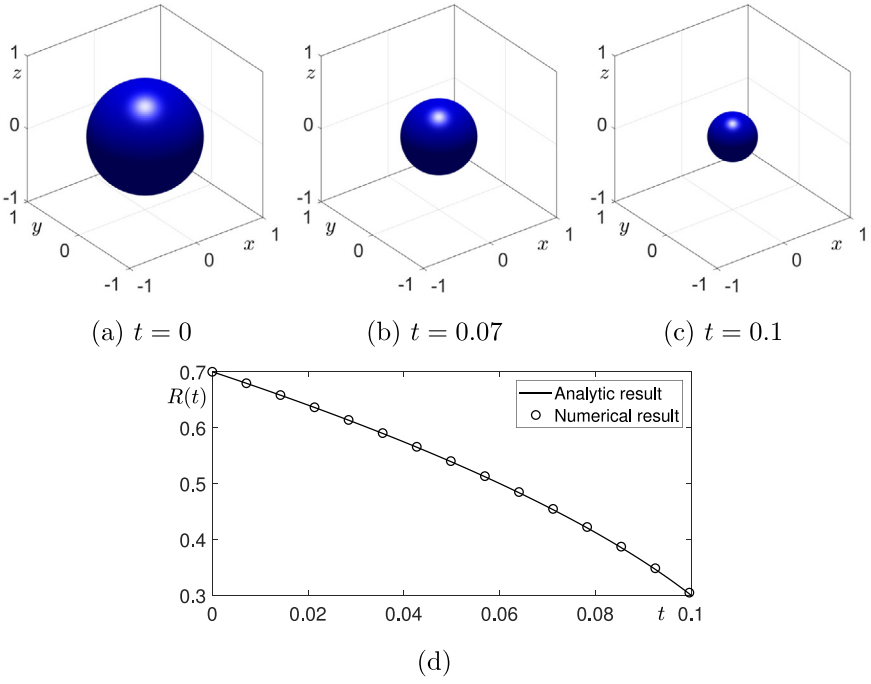

Fig. 7. (a)–(c) Temporal evolution of zero level isosurface of the numerical solutions. (d) Analytic and numerical radius changes over time.

radii over time t. From the results in Figs. 6 and 7, for the explicit scheme, the analyzed time step makes the scheme stable and the solutions follow the motion by mean curvature well.

4. Conclusions

A fully explicit finite difference scheme for the AC equation has a time step restriction, however, the numerical scheme is fast and accurate. In this study, we discussed the stability of a fully explicit finite difference scheme for solving the AC equation. We analyzed the stability of the fully explicit scheme for the AC equation and found optimal time step restrictions for the stability of the scheme in 1D, 2D, and 3D spaces. We confirmed the stability of the scheme with the analyzed time step restriction through the numerical experiments. In 1D space, using the traveling wave solution, we performed the convergence test and compared the accuracy with FSM. In 2D and 3D space, we investigated the mean curvature flow of the numerical solutions with the proposed time step restriction. In this paper, we focused on the polynomial free energy potential for the AC equation, however there exists a stability energy approach for the Flory–Huggins logarithmic potential on AC equation [27]. Furthermore, there are interesting future extensions of positivity-preserving property numerical analysis and applications with the Flory–Huggins free energy [8–10,35].

Declaration of competing interest

The authors declare that they have no known competing financial interests or personal relationships that could have appeared to influence the work reported in this paper.

Acknowledgment

The corresponding author (J.S. Kim) was supported by the National Research Foundation (NRF), Korea, under project BK21 FOUR. The authors would like to thank the reviewers for their valuable suggestions and comments to improve the paper.

References

[1] A.A. Aderogba, M. Chapwanya, An explicit nonstandard finite difference scheme for the Allen–Cahn equation, J. Difference Equ. Appl. 21 (10) (2015) 875–886.
[2] S.M. Allen, J.W. Cahn, A microscopic theory for antiphase boundary motion and its application to antiphase domain coarsening, Acta Metall. 27 (6) (1979) 1085–1095.
[3] A.L. Brkić, A. Novak, A nonlocal image inpainting problem using the linear Allen–Cahn equation, in: Conference on Non-Integer Order Calculus and Its Applications, Springer, Cham, 2018, pp. 229–239.
[4] W. Chen, C. Chen, X. Wang, S.M. Wise, Positivity-preserving, energy stable numerical schemes for the Cahn–Hilliard equation with logarithmic potential, J. Comput. Phys. X 3 (2019) 100031.
[5] J.W. Choi, H.G. Lee, D. Jeong, J. Kim, An unconditionally gradient stable numerical method for solving the Allen–Cahn equation, Physica A 338 (9) (2009) 1791–1803.
[6] M.I.M. Copetti, C.M. Elliott, Numerical analysis of the Cahn–Hilliard equation with a logarithmic free energy, Numer. Math. 63 (1) (1992) 39–65.
[7] J. Deteix, G.N. Kouamo, D. Yakoubi, A new energy stable fractional time stepping scheme for the Navier–Stokes/Allen–Cahn diffuse interface model, Comput. Methods Appl. Mech. Engrg. 393 (2022) 114759.
[8] L. Dong, C. Wang, S.M. Wise, Z. Zhang, A positivity-preserving, energy stable scheme for a ternary Cahn–Hilliard system with the singular interfacial parameters, J. Comput. Phys. 442 (2021) 110451.
[9] L. Dong, C. Wang, H. Zhang, Z. Zhang, A positivity-preserving, energy stable and convergent numerical scheme for the Cahn–Hilliard equation with a Flory–Huggins–Degennes energy, Commun. Math. Sci. 17 (4) (2019) 921–939.
[10] L. Dong, C. Wang, H. Zhang, Z. Zhang, A positivity-preserving second-order BDF scheme for the Cahn-Hilliard equation with variable interfacial parameters, Commun. Comput. Phys. 28 (3) (2020) 967–998.
[11] S. Geng, T. Li, Q. Ye, X. Yang, A new conservative Allen–Cahn type Ohta-Kawaski phase-field model for diblock copolymers and its numerical approximations, Adv. Appl. Math. Mech. 14 (1) (2022) 101–124.
[12] D. Jeong, J. Kim, An explicit hybrid finite difference scheme for the Allen–Cahn equation, J. Comput. Appl. Math. 340 (2018) 247–255.
[13] D. Jeong, S. Lee, D. Lee, J. Shin, J. Kim, Comparison study of numerical methods for solving the Allen–Cahn equation, Comput. Mater. Sci. 111 (2016) 131–136.
[14] D. Jeong, Y. Li, Y. Choi, C. Lee, J. Yang, J. Kim, A practical adaptive grid method for the Allen–Cahn equation, Physica A 573 (2021) 125975.
[15] V. Joshi, R.K. Jaiman, An adaptive variational procedure for the conservative and positivity preserving Allen–Cahn phase-field model, J. Comput. Phys. 366 (2018) 478–504.
[16] J. Kim, Adaptive mesh refinement for thin-film equations, J. Korean Phys. Soc. 49 (5) (2006) 1903.
[17] D.S. Lee, J.S. Kim, Mean curvature flow by the Allen–Cahn equation, European J. Appl. Math. 26 (4) (2015) 535–559.
[18] D. Lee, S. Lee, Image segmentation based on modified fractional Allen–Cahn equation, Math. Probl. Eng. 2019 (2019).

[19] Y. Li, D. Jeong, J.I. Choi, S. Lee, J. Kim, Fast local image inpainting based on the Allen–Cahn model, Digit. Signal Process. 37 (2015) 65–74.
[20] Y. Li, K. Qin, Q. Xia, J. Kim, A second-order unconditionally stable method for the anisotropic dendritic crystal growth model with an orientation-field, Appl. Numer. Math. 184 (2023) 512–526.
[21] Y. Li, Q. Xia, C. Lee, S. Kim, J. Kim, A robust and efficient fingerprint image restoration method based on a phase-field model, Pattern Recognit. 123 (2022) 108405.
[22] Y. Li, Q. Xia, S. Yoon, C. Lee, B. Lu, J. Kim, Simple and efficient volume merging method for triply periodic minimal structures, Comput. Phys. Comm. 264 (2021) 107956.
[23] K. Li, H. Zhang, Explicit Runge–Kutta scheme with high efficiency and energy dissipation for the Allen–Cahn equation, J. Phys. Conf. Ser. 1682 (1) (2020) 012031.
[24] Y. Li, L. Zhang, Q. Xia, Q. Yu, J. Kim, An unconditionally energy-stable second-order time-accurate numerical scheme for the coupled Cahn–Hilliard system in copolymer/homopolymer mixtures, Comput. Mater. Sci. 200 (2021) 110809.
[25] H. Montanelli, N. Bootland, Solving periodic semilinear stiff PDEs in 1D, 2D and 3D with exponential integrators, Math. Comput. Simulation 178 (2020) 307–327.
[26] T. Tang, J. Yang, Implicit-explicit scheme for the Allen–Cahn equation preserves the maximum principle, J. Comput. Math. (2016) 451–461.
[27] X. Wang, J. Kou, J. Cai, Stabilized energy factorization approach for Allen–Cahn equation with logarithmic Flory–Huggins potential, J. Sci. Comput. 82 (2) (2020) 1–23.
[28] X. Wang, J. Kou, H. Gao, Linear energy stable and maximum principle preserving semi-implicit scheme for Allen–Cahn equation with double well potential, Commun. Nonlinear Sci. Numer. Simul. 98 (2021) 105766.
[29] A.M. Wazwaz, The tanh-coth method for solitons and kink solutions for nonlinear parabolic equations, Appl. Math. Comput. 188 (2) (2007) 1467–1475.
[30] Q. Xia, J. Kim, B. Xia, Y. Li, An unconditionally energy stable method for binary incompressible heat conductive fluids based on the phase–field model, Comput. Math. Appl. 123 (2022) 26–39.
[31] Q. Xia, G. Sun, Q. Yu, J. Kim, Y. Li, Thermal-fluid topology optimization with unconditional energy stability and second-order accuracy via phase-field model, Commun. Nonlinear Sci. Numer. Simul. 116 (2023) 106782.
[32] X. Xiao, X. Feng, A second-order maximum bound principle preserving operator splitting method for the Allen–Cahn equation with applications in multi-phase systems, Math. Comput. Simulation (2022).
[33] J. Yang, D. Jeong, J. Kim, A fast and practical adaptive finite difference method for the conservative Allen–Cahn model in two-phase flow system, Int. J. Multiph. Flow 137 (2021) 103561.
[34] S. Yoon, D. Jeong, C. Lee, H. Kim, S. Kim, H.G. Lee, J. Kim, Fourier-spectral method for the phase-field equations, Mathematics 8 (8) (2020) 1385.
[35] M. Yuan, W. Chen, C. Wang, S.M. Wise, Z. Zhang, An energy stable finite element scheme for the three-component Cahn–Hilliard-type model for macromolecular microsphere composite hydrogels, J. Sci. Comput. 87 (3) (2021) 1–30.